Stress-induced structural changes in electrospun polyvinylidene difluoride nanofibers collected using a modified rotating disk

Wu Aik Yee [a], Anh Chien Nguyen [a], Pooi See Lee [a], Masaya Kotaki [b], Ye Liu [c], Boon Teoh Tan [a], Subodh Mhaisalkar [a], Xuehong Lu [a,*]

[a] School of Materials Science and Engineering, Nanyang Technological University, 50 Nanyang Avenue, Singapore 639798
[b] Division of Advanced Fibro Science, Kyoto Institute of Technology, Matsugasaki, Sakyo-ku, Kyoto 606-8585, Japan
[c] Institute of Materials Research and Engineering, 3 Research Link, Singapore 117602

ARTICLE INFO

ABSTRACT

By attaching separate, parallel electrodes onto a rotating disk collector, well aligned electrospun polyvinylidene difluoride (PVDF), PVDF/carbon nanotube nanocomposite and vinylidene fluoride–trifluoroethylene copolymer nanofibers are directly deposited onto flat substrates forming relatively large, uniform and compact fibrous thin films. The attachments alter the electric-field distribution on the rotating disk, which fosters the fanning of the nanofibers, while the electric field between the separate electrodes and the mechanical force exerted by the rotational disk facilitate the alignment. X-ray diffraction and infrared spectroscopic studies show that the specific environment and force fields created on the modified rotating disk cause the electrospun fibers being effectively stretched to form highly oriented β-form crystallites with slightly reduced inter-chain distance. They also lead to slight increases in crystallinity and crystal size. A mechanism is proposed to account for the structural alteration induced by the modified rotating disk collector. Ferroelectricity of the aligned electrospun PVDF fibrous thin films is also demonstrated.

© 2008 Elsevier Ltd. All rights reserved.

1. Introduction

Polyvinylidene difluoride (PVDF) is an attractive material for many applications due to its electroactive properties as well as light weight, flexibility and good electrochemical stability. Depending on processing conditions, PVDF can exhibit at least four distinct polymorphs, which involve three different chain conformations, namely (1) slightly twisted all-*trans* zigzag (*TTTT*, *T* denotes *trans*) for β-phase, (2) *TGTG'* (*G* denotes *gauche*) for α and δ (α_p) phases and (3) *TTTGTTTG'* for γ phase [1,2]. Folded-chain crystals are formed in PVDF under common conditions, while under high pressure and temperature PVDF can also form β-form extended-chain crystals [3]. When PVDF chains are packed into crystal lattices, their dipoles are either additive, which leads to a net dipole as in β, γ and α_p phases, or subtractive, resulting in no net dipole as in α-phase. Among the three polar polymorphs, the β-form has the largest spontaneous polarization per unit cell and exhibits the highest piezo- and ferroelectric activities [1]. In piezoelectric and ferroelectric thin film devices, the direction of the polarizing electric field is normally perpendicular to the film surface. If the *c*-axis

of the β-crystallites are oriented parallel to the film surface, the dipoles of the all-*trans* conformers will be in the *b*-axis direction of the orthorhombic lattice, which can be easily aligned along the normal of the thin film by the applied electric field. Preferred crystal orientation in PVDF can be achieved via melt spinning [4] or extrusion [5], mechanical drawing [6], Langmuir–Blodgett deposition [7] and poling [8,9]. An alternative route discovered recently is electrospinning, which promotes both the formation of the β-phase [10–12] and preferred crystal orientation [11].

Electrospinning has received great attention in the past few years due to its simplicity, inexpensiveness and versatility for fabrication of nanofibers. In particular, enormous research efforts have been devoted to the creation of aligned two-dimensional (2D) nanofiber assemblies for various emerging applications [13]. A common approach for the alignment of electrospun fibers is to use rotating apparels such as a drum or disk to collect preferentially aligned fibers in the rotating direction [14,15]. With the rotating disk, highly aligned fibrous thin films can, however, only be obtained in a very small area around the tip of the blade, which is insufficient for device applications. With the rotating drum, large-area collection of preferentially aligned electrospun fibers is possible but the quality of the alignment is not as good as that achieved with the rotating disk. Good alignment of electrospun fibers has also been demonstrated when the fibers are collected in

---

* Corresponding author. Tel.: +65 6790 4585; fax: +65 6790 9081.
  E-mail address: asxhlu@ntu.edu.sg (X. Lu).

the air gap between two static parallel electrodes due to the residual electrostatic repulsion between the electrospun fibers [16], whereas the transfer of the nanofiber assemblies onto a solid substrate usually causes fiber breakage, especially for weak polymeric nanofibers. In a recent publication, we reported that electrospinning of PVDF can lead to the formation of the β-phase significantly and the c-axis of the β-crystallites can be preferably aligned along the fiber axis via the collection using a conventional rotating disk [11]. The aligned fibrous thin films have however a very small area (submicron scale). In this paper, we report the direct deposition of well-aligned electrospun fibrous thin films of PVDF-based polymers uniformly onto a relatively large flat substrate (centimeter scale) using a simple set-up, i.e. a modified rotating disk collector. Our modification is similar to some modified rotating collectors in terms of utilizing both electric field and mechanical force to align the fibers [17]; however, instead of the addition of auxiliary electrodes, our modified rotating disks have separate, parallel electrodes attached on the rotating disk, which can stretch the fibers in the air gap between the separate electrodes effectively. The influences of the combined force fields on morphology, crystal structure and orientation of the polymers are discussed in this paper. Ferroelectricity of the aligned 2D nanofiber assemblies is also demonstrated.

2. Experimental

2.1. Materials

PVDF powders (Solef 11008) and vinylidene difluoride–trifluoroethylene copolymer (P(VDF-TrFE), 70/30 mol%) pellets were used as received. Multi-walled carbon nanotube (MWCNT) of ∼10 nm diameter was purchased from Catalytic Materials Ltd. and functionalized via treating with sulfuric and nitric acids [18]. N,N-Dimethylformamide (DMF) and acetone were supplied by Aldrich.

2.2. Electrospinning

A DMF/acetone mixture was prepared at the DMF/acetone weight ratio of 60/40. PVDF and P(VDF-TrFE) were then dissolved in the solvent mixture at the polymer/solvent weight ratio of 20/100. A solution was also made by mixing 0.01 wt.% functionalized MWCNT with PVDF in the solvent mixture. The polymer solutions were placed in a plastic syringe fitted with a needle of tip-diameter 200 μm. Electrospinning was conducted at 15 kV with a high-voltage power supply. A syringe pump was used to feed the polymer solutions into the needle tip at the rate of 0.25 ml/h. The electrospun fibers were collected using the conventional (unmodified) and modified rotating disks, as shown in Fig. 1, at the rotating speed of 1500 rpm for 1 h. The modified rotating disk (Fig. 1b) has separate, parallel aluminum plates with sharp edges attached on the unmodified rotating disk. Grounded flat substrates, such as indium tin oxide (ITO) glass or silicon wafer, of 25 mm × 20 mm ($X \times Y$) were placed between the aluminum plates to collect the aligned electrospun fibers in the rotation direction. Static separate electrodes [15] were also used to collect the nanofibers electrospun under the same conditions to make reference samples. All the collectors were placed at a distance of 15 cm below the needle. All electrospun fibers were dried in vacuo at room temperature overnight prior to characterization.

2.3. Characterization

All samples were characterized via wide angle X-ray diffraction (WAXD) using Cu Kα radiation (0.154 nm) generated at 40 kV and 40 mA, attenuated Fourier transform infrared (FTIR) spectroscopy and differential scanning calorimetry (DSC). The instruments and
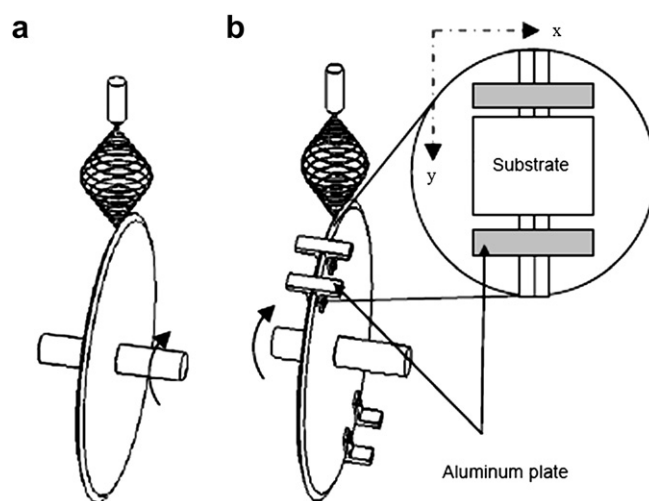

Fig. 1. Schematics showing the electrospinning process using (a) a conventional rotating disk collector and (b) the modified rotating disk collector.

conditions for the characterization were the same as that reported in Ref. [11]. To assess the orientation states of the crystallites of different structures, the two-dimensional (2D) WAXD patterns obtained were divided into four regions in the 2θ range of $18°–23°$, i.e. $18°–19°$, $19°–20°$, $20°–21°$ and $21°–23°$ 2θ. In each region the radial-average intensity was determined using the GADDS software package to obtain the intensity versus azimuthal angle plot. The resolution for the FTIR scans was $4.0\,\mathrm{cm}^{-1}$, and the curves were normalized by setting the intensity of the band at $1070\,\mathrm{cm}^{-1}$, which is insensitive to phase changes, to a constant value. For all the samples, DSC measurements were repeated five times and an average was taken.

2.4. Polarization measurement

The fibrous thin films were sandwiched between a thin piece of aluminum plate and a copper strip covered with a glass slide. The assembly was clamped tightly together using Hoffman clamps. The polarization was then measured using a Radiant Technology RT6000HVS polarization tester. A total of 20 measurements were taken for signal averaging. Film thickness was measured using an Elcometer 456 equipped with probe T456F1S.

3. Results and discussion

3.1. The aligning process

During the electrospinning, it can be clearly observed that the modified rotating disk leads to fanning of the electrospun fibers as they approach the aluminum plates, as shown in Fig. 2. The reason is that the conductive aluminum electrodes on the disk effectively reduce the strength of the electric field on the tip of the disk [19] and hence foster the electrospun fibers to whip in the directions off the tip of the disk. The fanning process promotes solvent evaporation so that the electrospun fibers may subsequently be more effectively stretched at a high-viscosity state when crossing the gap between the separate electrodes on the disk. The impact of this on crystalline structures and orientation of the polymers will be discussed in Section 3.2.

3.2. Crystal structures and orientation

In this work, PVDF fibrous thin films were fabricated via four different routes, namely, collected (1) on an ITO substrate between
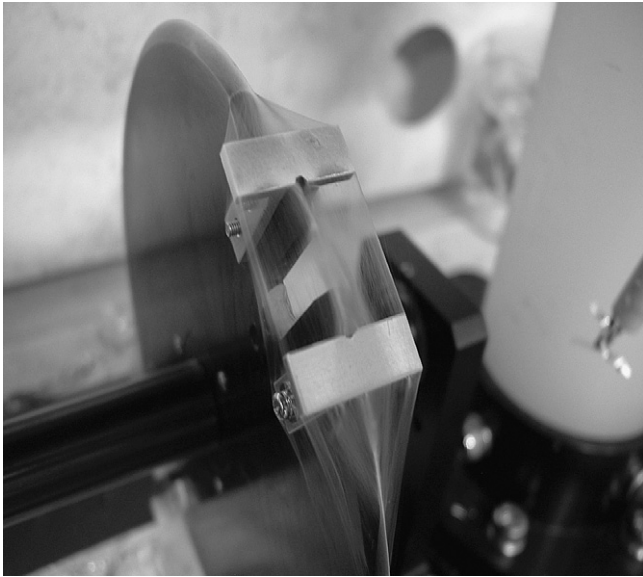
Fig. 2. A picture showing the fanning of the electrospun PVDF fibers on the modified rotating disk collector. No substrates were placed between the two aluminum electrodes.

Unit cell of the β modification of PVDF with a slightly deflected planar-zigzag conformation without stress

Unit cell of the β modification of PVDF with a more perfect planar-zigzag conformation under tensile stress

Fig. 4. A qualitative scheme illustrating the proposed structural change for the β-form crystal.

static separate electrodes, (2) in the air gap between the static separate electrodes, (3) using the unmodified rotating disk and (4) using the modified rotating disk. With route (2), (3) or (4), aligned electrospun PVDF fibrous thin films can be directly deposited or transferred onto a solid substrate, while route (1) gives a random mat on the substrate. For convenience, the four types of fibrous thin films will be named as sample a, b, c and d, respectively, in the rest of the paper. A detailed comparison among the morphologies of the four samples will be discussed in the Section 3.3. In this section, we will focus on the crystalline structural changes induced by the modified rotating disk collector.

WAXD patterns and FTIR spectra of the four samples are shown in Fig. 3A and B, respectively. For the sample a (the random mat), a strong diffraction peak at $2\theta = 20.5°$, which corresponds to the sum of the 110 reflection of the α-phase and 200/110 reflections of the β-phase, and distinctive peaks at around 18.5 and 27.4° 2θ, which correspond to 020 and 021 reflections of the α-phase, respectively, indicate the co-existence of the α- and β-phases [20]. This is corroborated by its FTIR spectrum (curve a) where the α-phase related bands can be observed at 614, 765, 795 and 975 cm^{-1} and the β-phase related bands at 840 and 1278 cm^{-1} [21]. The samples b and c, although being aligned ones, show similar diffraction patterns and infrared spectra to those of the sample a, while for the sample d a shoulder peak appears at around 22° 2θ
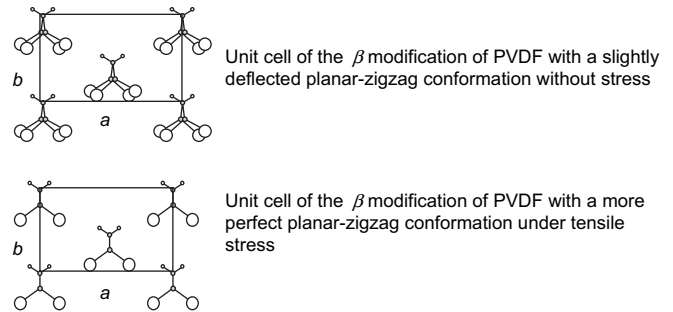
despite that its infrared spectrum remains similar to that of the others. The shoulder peak at 22° 2θ is an equatorial peak and can also be assigned as the 200/110 reflections of the β-phase, which indicates that although the use of the modified rotating disk collector does not have a significant β-phase enhancement effect, it leads to the formation of the β-form crystallites with slightly reduced inter-chain distance. A hypothetic mechanism for the formation of such a structure via the use of the modified rotating disk collector is that the fast solvent evaporation during the fanning may create a specific high-viscosity environment where a tensile stress could be effectively loaded onto polymer chains when the fibers are stretched between the two electrodes by the electric field and mechanical force, whereas the polymer chains could still pack to crystallize through "sliding diffusion" [22] to form extended-chain crystals. By tubular film extrusion and drawing, fibril crystals can be nucleated in PVDF [5] so that it is not surprising that they may also form in highly stressed electrospun fibers. Under the tensile stress, the slightly twisted zigzag conformation based on energy minimization without stress [1,2] may become a more perfect planar-zigzag, which may make slightly smaller lattice parameter(s) possible, as illustrated in Fig. 4. Since WAXD reflects the development of long-range order whereas FTIR measures local conformational changes [23], the structure change could only be observed via WAXD probably because the conformational change is too small to be detected by FTIR.

Further justification for the mechanism proposed above can be found through comparing the orientation states of the crystallites of different structures. In order to differentiate the orientation states of the electrospun PVDF fibers collected using the modified and unmodified rotating disk collector (the samples c and d), their 2D WAXD patterns were divided into four regions in the 2θ range of 18°–23°, i.e. $2\theta = 18°–19°$ (I), 19°–20° (II), 20°–21° (III) and 21°–23° (IV), and each region was separately scanned to obtain radial-average intensity versus azimuthal angle plots. Fig. 5a shows the
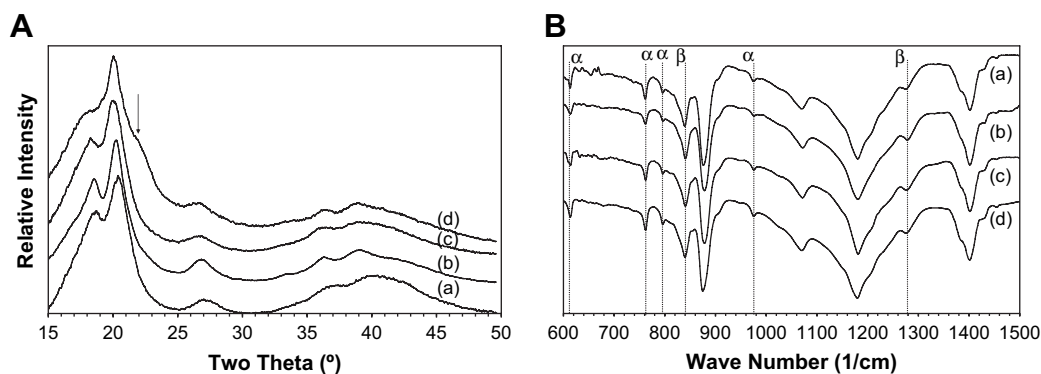

Fig. 3. (A) WAXD patterns and (B) FTIR spectra of electrospun PVDF fibrous thin films collected using (a) the static separate electrodes on an ITO substrate, (b) the static separate electrodes in the air gap, (c) the unmodified rotating disk and (d) the modified rotating disk.

azimuthal-average intensity versus 2θ plots for the two samples, which illustrates how the WAXD patterns are divided into four regions. The intensity in the regions I and II is mainly from the α-form crystallites (reflections 100 and 020), while the intensity in the regions III and IV is dominantly contributed by the β-form crystallites (reflections 110 and 200). Furthermore, based on our hypothesis, the region III corresponds to the β-form crystallites formed under normal electrospinning conditions, while the region IV corresponds to the extended-chain β-form crystallites formed under high tensile stress. Fig. 5b shows the radial-average intensity versus azimuthal angle (χ) plots for the four regions obtained from the 2D WAXD patterns (c.f. Supporting information for the 2D patterns). For the regions I and II (Fig. 5b(i) and (ii)), the peaks for the modified rotating disk appear slightly sharper than the ones for its unmodified counterpart, indicating that the modified rotating disk gives a slightly higher degree of orientation to the α-phase than the unmodified rotating disk. A similar trend is observed for the region III (Fig. 5b(iii)). It is also evident that the peaks for the region III are slightly sharper than the corresponding peaks for the

regions I and II, suggesting that the "normal" β-phase has a slightly higher degree of orientation than the α-phase regardless of which rotating disk is used. For the region IV (Fig. 5b(iv)), a much shaper peak is, however, observed for the modified rotating disk, indicating that the stress-induced β-form crystallites are highly oriented. The above facts reveal that the tensile stress that is experienced by the nanofibers when crossing the separate electrodes on the modified rotating disk influences the orientation of both the α- and β-form crystallites significantly. Moreover, they prove the formation of stress-induced β-form crystallites, which have not only a smaller inter-chain distance but also a much higher degree of orientation than the "normal" β-form crystallites.

To confirm that the diffraction peak at 22° 2θ is indeed from the β-form crystallites induced by the modified rotating disk collector, 0.01 wt.% MWCNT is dispersed into PVDF solution to produce β-phase-dominant electrospun fibers [24]. The WAXD patterns and FTIR spectra of PVDF/MWCNT fibrous thin films obtained using the unmodified and modified rotating disk collectors, which are named as sample e(i) and e(ii), respectively, are shown in Fig. 6. The
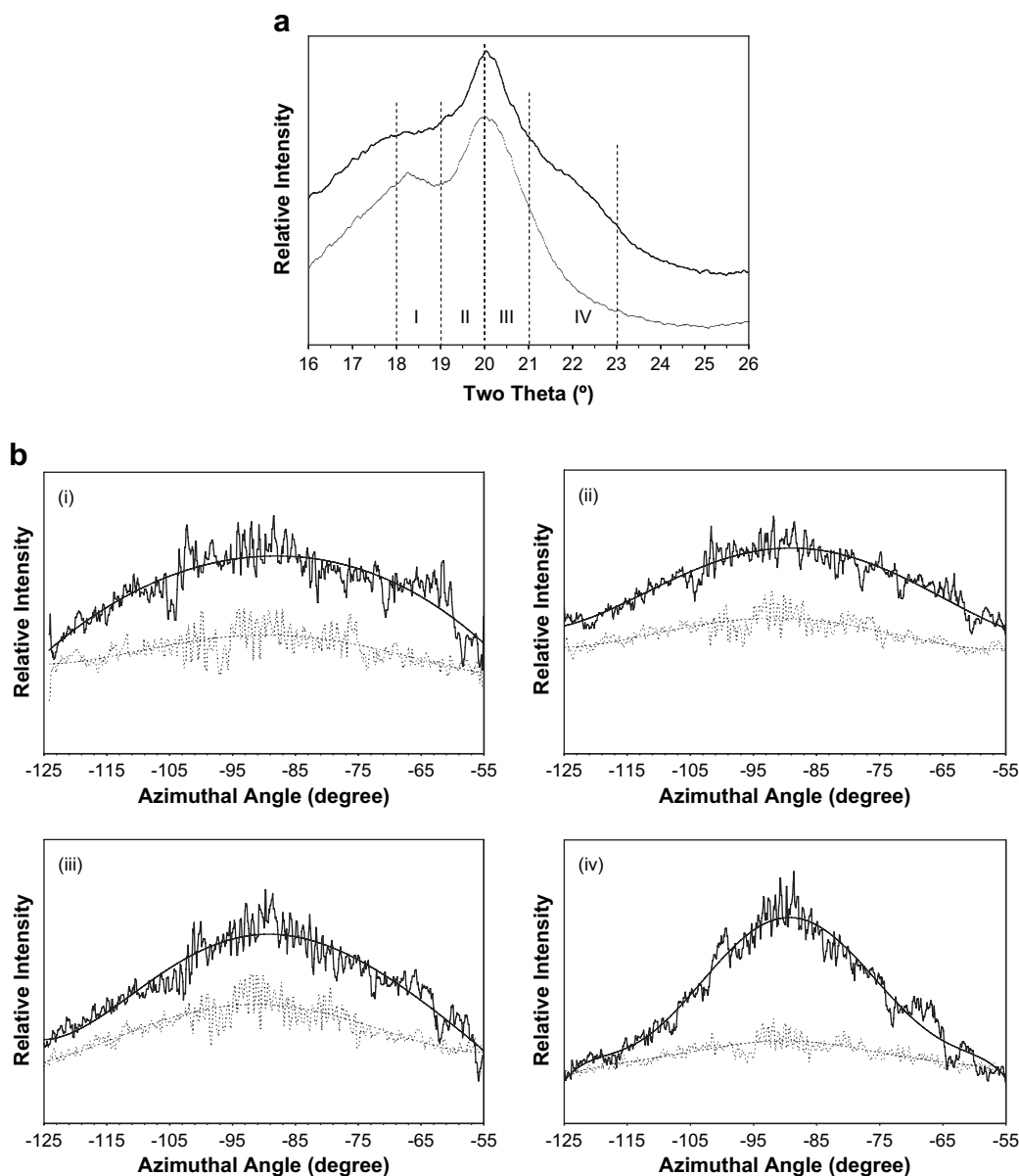

Fig. 5. (a) Azimuthal-average intensity versus 2θ plots and (b) radial-average intensity versus azimuthal angle plots obtained by scanning the 2D WAXD patterns of PVDF nanofibers collected using the modified (solid line) and the unmodified rotating disk (dashed line) for the region (I) $2\theta = 18^{\circ}-19^{\circ}$, (II) $2\theta = 19^{\circ}-20^{\circ}$, (III) $2\theta = 20^{\circ}-21^{\circ}$ and (IV) $2\theta = 21^{\circ}-23^{\circ}$.
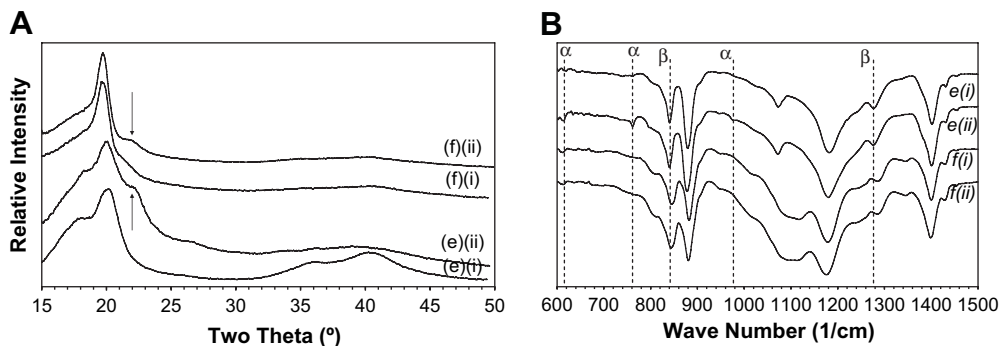
Fig. 6. (A) WAXD patterns and (B) FTIR spectra of the aligned electrospun (e) PVDF/MWCNT and (f) P(VDF-TrFE) fibrous thin films collected using (i) the unmodified rotating disk and (ii) the modified rotating disk.

absence of any diffraction peak at around 27° 2θ for the sample e(i) (curve e(i) in Fig. 6A) indicates that the β-phase is dominant in this sample. This is corroborated by its FTIR spectrum (curve e(i) in Fig. 6B) in which no α-phase band can be seen. For the sample e(ii), a fairly strong shoulder peak appears at 22° 2θ (curve e(ii) in Fig. 6A), while its FTIR spectrum (curve e(ii) in Fig. 6B) again shows no significant enhancement of the β-phase compared with the sample e(i). Fig. 7 shows the 2D WAXD patterns of the samples e(i) and e(ii). Clearly, the equatorial peak at 22° 2θ for the sample e(ii) corresponds to the crystallites highly oriented along the fiber axis, which supports the hypothesis that this peak arises from the crystals induced by the tensile stress in the fiber direction. The stronger diffraction peak at 22° 2θ for the sample e(ii) as compared to the sample d (PVDF) can be attributed to the interactions between the MWCNT and PVDF chains [25] that may promote the chain orientation further. Some weak α-phase infrared bands are also observed from the sample e(ii), which could be attributed to the tensile stress exerted by the modified rotating disk collector that also promotes the α-phase slightly. The unmodified and modified rotating disk collectors are also used to collect electrospun P(VDF-TrFE) nanofibers (sample f(i) and f(ii)). The ferroelectric phase (similar to the *all-trans* β-phase in PVDF) is obtained with both the unmodified and modified rotating disk collectors as no diffraction peak and infrared band for the paraelectric phase (similar to the α-phase in PVDF) are observed (Fig. 6A(f) and Fig 6B(f)). More importantly, the use of the modified rotating disk

collector also leads to a distinct diffraction peak at around 22° 2θ for P(VDF-TrFE) (Fig. 6A(f)(ii)). The consistent trend observed from PVDF, PVDF/MWCNT and P(VDF-TrFE) confirms that the diffraction peak at 22° 2θ is a characteristic of the β/ferroelectric phase obtained in the specific environment created on the modified rotating disk collector. It is worth noting that in this work the WAXD patterns were obtained by placing highly aligned electrospun fibers perpendicular to the X-ray beam so that meridional and some off-equator peaks are very weak. The verification of the proposed crystalline structure and superstructure requires further experimental studies and molecular simulation, which are beyond the scope of this work.

Table 1 lists the results of DSC measurements (c.f. DSC curves in Supporting information). It shows that the use of the modified rotating disk also leads to a slight increase in peak melting temperature and heat of fusion, which signifies slightly increased crystal size and crystallinity due to the stretching of the nanofibers. The increased crystallinity for PVDF and PVDF/MWCNT may come from both the α and β-phases as from the WAXD patterns and FTIR spectra of the sample d and e(ii) we can observe very slight enhancement of the α-phase as compared with the sample c and e(i). The melting temperatures of the fibrous thin films collected using the modified rotating disk are only marginally higher than that from the unmodified rotating disk but much lower than that of the β-form extended-chain crystals obtained under high-pressure conditions [3], which is probably due to the much smaller crystal size in the nanofibers.
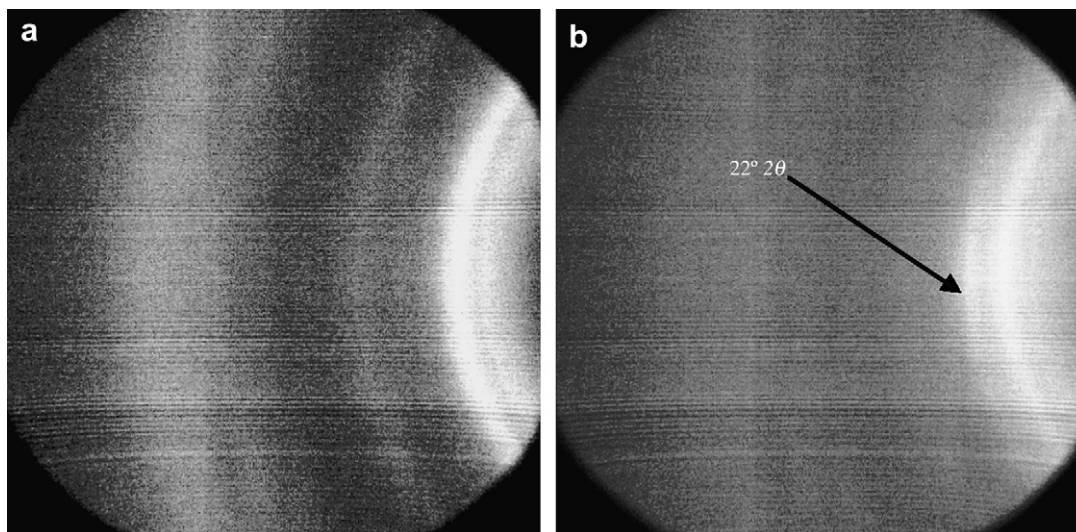

Fig. 7. 2D WAXD patterns of the electrospun PVDF/MWCNT fibrous thin films obtained using (a) the unmodified rotating disk and (b) modified rotating disk collector.

Table 1
Heat of fusion and peak melting temperatures obtained from the first heating DSC curves of the aligned electrospun fibrous thin films using the modified and unmodified rotating disk collector

Material	Collector	Heat of fusion (J/g)	Melting temperature (°C)
PVDF	Unmodified rotating disk	42.5 ± 1.6	157.1 ± 0.3
PVDF	Modified rotating disk	46.2 ± 1.3	157.5 ± 0.5
PVDF/MWCNT	Unmodified rotating disk	42.3 ± 1.9	157.4 ± 0.2
PVDF/MWCNT	Modified rotating disk	44.2 ± 1.2	158.1 ± 0.2
P(VDF-TrFE)	Unmodified rotating disk	33.5 ± 1.0	152.8 ± 0.3
P(VDF-TrFE)	Modified rotating disk	34.4 ± 1.1	152.9 ± 0.2

3.3. Morphology of the 2D nanofiber assemblies

It is found that although the degree of alignment of the electrospun fibers collected using the modified and unmodified rotating disks is about the same (Fig. 8a and b), the lateral distribution of the fibers on the centimeter-sized substrates is very different for these two methods (Fig. 9a and b). For the modified rotating disk, the specific electric-field distribution created by attaching the aluminum electrodes, coupled with the repelling force from the residual charges on the electrospun fibers, gives rise to a uniform deposition of the electrospun fibers on the flat substrates across a relatively large distance (25 mm) in the lateral direction (Fig. 9a), while in the longitudinal direction the electric field between the two parallel electrodes, coupled with the mechanical force exerted by the rotating disk, ensures good alignment of the electrospun fibers after the fanning, as shown in Fig. 8a.

In contrast, a uniform lateral distribution of electrospun fibers cannot be achieved when ITO substrates are attached on the
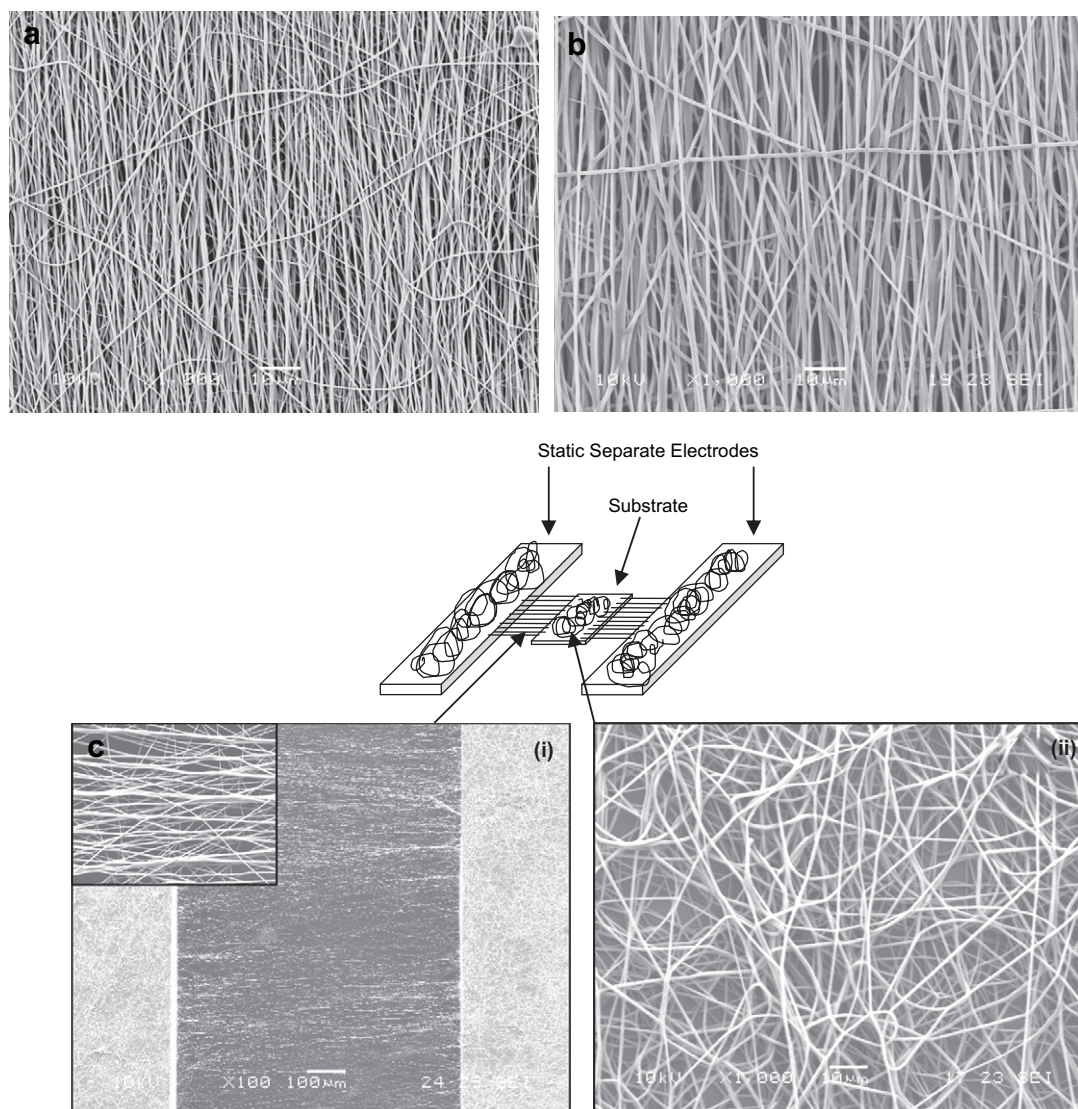

Static Separate Electrodes

Substrate

Fig. 8. SEM micrographs showing the morphologies of the electrospun P(VDF-TrFE) fibrous thin films obtained using (a) the modified rotating disk collector, (b) the unmodified rotating disk collector and (c) static separate electrodes. In (c), (i) shows the morphology of the aligned fibers in the gaps between the static separate electrodes and the substrate while (ii) shows the morphology of the random mat on the substrate.
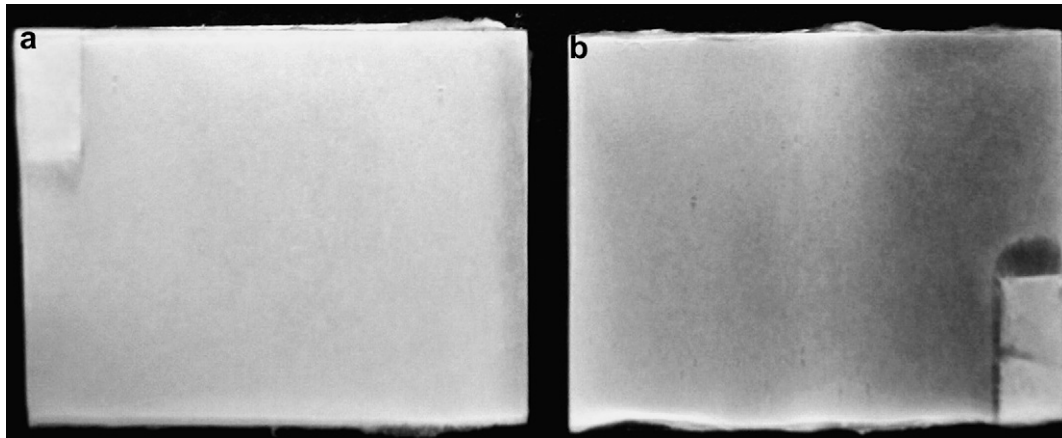
Fig. 9. A picture showing electrospun P(VDF-TrFE) fibrous thin films collected on ITO substrates using (a) the modified rotating disk collector and (b) the unmodified rotating disk collector. In (b) the central area is whiter than the two sides because of the low density of the electrospun fibers on the two sides.

unmodified disk, as shown in Fig. 9b. For the static separate electrodes with a substrate in between, the alignment of the electrospun fibers can only be observed in the air gaps between the electrodes (Fig. 8ci) and the substrate, while on the substrates the fibers form a random mat (Fig. 8cii). The transferring of the aligned fibrous thin films in the air gap onto a substrate causes the breakage of weak fibers, especially when the distance between the two electrodes is large. Obviously, static separate electrodes are unsuitable for the direct deposition of aligned electrospun fibers onto conductive substrates. Compared with the static separate electrodes, the modified rotating disk collector is also able to provide good alignment in a longer (in the fiber axis direction) and thicker sample, and improves the compactness of the fibrous thin films due to the mechanical force exerted by the rotating disk, which enables the ferroelectric testing of the thin films.

3.4. Ferroelectricity of the thin films

To demonstrate ferroelectricity of the electrospun PVDF nanofibers, polarization of the PVDF fibrous thin film was measured, with P(VDF-TrFE) and PVDF/P(VDF-TrFE) blends electrospun under the same conditions as references. In the measurements, polarization saturation could not be achieved due to short circuiting at high E values. Nevertheless, $P–E$ hysteresis loops were obtained at relatively low voltages, as shown in Fig. 10. Moreover, the

polarization achieved at the maximum E clearly increases with the PVDF content in the blends. Since PVDF and P(VDF-TrFE) do not co-crystallize [26], the composition dependence of the polarization suggests that the macroscopic polarization observed at the maximum E is mainly caused by constituent dipoles of the polymers rather than the trapped charges. Thus, the hysteresis loops provide direct evidence for the switching of the dipoles in the electrospun PVDF nanofibers although there are trapped charges in the thin films as indicated by a gain at the voltage of zero as compared with that at the maximum voltage applied. The charge trapping could be attributed to the fibrous nature of the films, which inevitably resulted in some voids. This is also the main reason why polarization saturation could not be achieved. It is worth noting that PVDF exhibits higher polarizability than the copolymer when processed using this unique method, which may be attributed to the much higher crystallinity of the PVDF nanofibers and the larger dipole moment of the β-phase of PVDF than that of the β-phase of P(VDF-TrFE) per unit cell. The ferroelectricity of electrospun PVDF/MWCNT fibrous thin films could not be tested as 0.01 wt.% MWCNT has reached the conduction threshold.

4. Conclusions

Using the modified rotating disk collector, the direct deposition of well-aligned electrospun PVDF nanofibers with relatively good compactness and uniformity across a relatively large flat substrate is achieved. The modification alters the electric-field distribution on the disk, which fosters the fanning of the nanofibers, while the electric field between the separate electrodes and the mechanical force exerted by the rotational disk facilitate the alignment. The specific environment and force fields created on the modified rotating disk cause the electrospun fibers being effectively stretched to form highly oriented β-form crystallites with slightly reduced inter-chain distance. It also leads to slight increases in crystallinity and crystal size. A hypothetic mechanism for the structural alteration is proposed: it may be related to the formation of extended-chain crystals with a more perfect planar-zigzag conformation under a high tensile stress. The $P–E$ hysteresis loops obtained from aligned PVDF fibrous thin films provide direct evidence for the switching of the dipoles in the electrospun PVDF nanofibers.
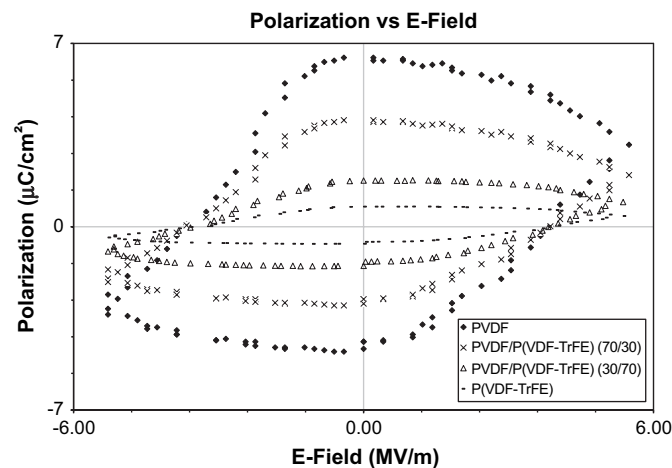

Fig. 10. Hysteresis loops obtained from the aligned electrospun fibrous thin films of PVDF, P(VDF-TrFE) and PVDF/P(VDF-TrFE) blends. All were collected using the modified rotating disk collector.

Appendix. Supporting information

Supplementary data associated with this article can be found in the online version, at doi:10.1016/j.polymer.2008.07.032.

References

[1] Tashiro K. In: Nalwa HS, editor. Ferroelectric polymers: chemistry, physics and applications. New York: Marcel Dekker Inc; 1995 [chapter 2].
[2] Wang ZY, Fan HQ, Su KH, Wen ZY. Polymer 2006;47:7988.
[3] Hattori T, Watanabe T, Akama S, Hikosaka M, Ohigashi H. Polymer 1997; 38:3505.
[4] Samon JM, Schultz JM, Hsiao BS. Polymer 2002;43:1873.
[5] Xu JN, Johnson M, Wilkes GL. Polymer 2004;45:5327.
[6] Branciforti MC, Sencadas V, Lanceros-Mendez S, Gregorio R. J Polym Sci Part B Polym Phys 2007;45:2793.
[7] Bune AV, Fridkin VM, Ducharme S, Blinov LM, Palto SP, Sorokin AV, et al. Nature 1998;391:874.
[8] Zhang H, Ren P, Zhang GF, Xiao CF. High Perform Polym 2006;18:305.
[9] Nguyen AC, Lee PS, Yee WA, Lu X, Srinivasan M, Mhaisalkar SG. J Electrochem Soc 2007;154:224.
[10] Nasir M, Matsumoto H, Minagawa M, Tanioka A, Danno T, Horibe H. Polym J 2007;39:670.
[11] Yee WA, Kotaki M, Liu Y, Lu X. Polymer 2007;48:512.
[12] Zheng J, He A. Macromol Rapid Commun 2007;28:2159.
[13] Teo WE, Ramakrishna S. Nanotechnology 2006;17:R89.
[14] Inai R, Kokaki M, Ramakrishna S. Nanotechnology 2005;16:208.
[15] Matthews JA, Wnek GE, Simpson DG, Bowlin GL. Biomacromolecules 2002; 3:232.
[16] Li D, Wang Y, Xia Y. Nano Lett 2003;3:1167.
[17] Wu Y, Carnell LA, Clark RL. Polymer 2007;48:5653.
[18] Yu X, Rajamani R, Stelson KA, Cui T. Sensors and Actuators A 2006;132:626.
[19] Sundaray B, Subramanian V, Natarajan TS, Xiang RZ, Chang CC, Fann WS. Appl Phys Lett 2004;84:1222.
[20] Newmann BA, Scheinbeim JI. Macromolecules 1983;16:60.
[21] Bormashenko Y, Pogreb R, Stanevsky O, Bormashenko E. Polym Test 2004;23: 791.
[22] Hikosaka M. Polymer 1990;31:458.
[23] Chua YC, Lu X. Langmuir 2007;23:1701.
[24] Levi N, Czerw R, Xing SY, Iyer P, Carroll DL. Nano Lett 2004;4:1267.
[25] Owens FJ, Jayakody JRP, Greenbaum SGC. Compos Sci Technol 2006; 66:1280.
[26] Gregorio R, Chaud MR, Santos WND, Baldo JB. J Appl Polym Sci 2002;85:1362.